Lighting Up DNA with the Environment-Sensitive Bright Adenine Analogue qAN4

ChemPubSoc Europe

DOI: 10.1002/cplu.201900712

CHEMPLUSCHEM Full Papers

Fb3

Lighting Up DNA with the Environment-Sensitive Bright Adenine Analogue qAN4

Anders F. Füchtbauer,[a] Moa S. Wranne,[a] Sangamesh Sarangamath,[a] Mattias Bood,[b, e] Afaf H. El-Sagheer,[c, d] Tom Brown,[c] Henrik Gradén,[e] Morten Grøtli,[b] and L. Marcus Wilhelmsson*[a]

The fluorescent adenine analogue qAN4 was recently shown to possess promising photophysical properties, including a high brightness as a monomer. Here we report the synthesis of the phosphoramidite of qAN4 and its successful incorporation into DNA oligonucleotides using standard solid-phase synthesis. Circular dichroism and thermal melting studies indicate that the qAN4-modification has a stabilizing effect on the B-form of DNA. Moreover, qAN4 base-pairs selectively with thymine with mismatch penalties similar to those of mismatches of adenine. The low energy absorption band of qAN4 inside DNA has its peak around 358 nm and the emission in duplex DNA is partly quenched and blue-shifted (ca. 410 nm), compared to the monomeric form. The spectral properties of the fluorophore also show sensitivity to pH; a property that may find biological applications. Quantum yields in single-stranded DNA range from 1–29% and in duplex DNA from 1–7%. In combination with the absorptive properties, this gives an average brightness inside duplex DNA of 275 $M^{-1}cm^{-1}$, more than five times higher than the most used environment-sensitive fluorescent base analogue, 2-aminopurine. Finally, we show that qAN4 can be used to advantage as a donor for interbase FRET applications in combination with adenine analogue qA_{nitro} as an acceptor.

Introduction

Nucleic acids are vital in the biology of cells. In understanding their interaction with other molecules, investigation of their structure and dynamics are essential. NMR,[1] X-ray crystallography[2] and lately also Cryo-EM[3] are frequently used for determining structure. However, drawbacks of these techniques are, for example, that NMR requires high sample concentrations while X-ray crystallography requires crystals, which are not always easy to form. Also, the fact that the crystal structure is encased in a crystal lattice with concomitant intermolecular interactions, and does not represent a free molecule in solution is a drawback. Despite generally offering a lower resolution, fluorescence techniques like Förster resonance energy transfer (FRET) can effectively complement these techniques, especially since fluorescence techniques have significant advantages when studying dynamics as well as large nucleic acid containing systems.[4] Moreover, FRET allows measurements to be performed inside living cells, which is an advantage compared to the other techniques.

To take advantage of the sensitivity and versatility of fluorescence spectroscopy for investigating the otherwise non-emissive nucleic acids, fluorescence labelling is required.[5] This can be done through external fluorescent dyes (*e.g.* Cy-, Alexa-, ATTO-dyes), non-covalently bound dyes, internal base stacking aromatic systems[6] or through fluorescent base analogues (FBAs).[7] In general, the latter group is less bright but has the advantage of being less perturbing, giving the possibility of being inserted close to the site of interest. FBAs normally also have the capacity for selective base-pairing and have a rigid and well-defined position within the nucleic acid. The latter two properties make FBAs particularly useful for measuring fluorescence anisotropy and FRET – techniques that reveal structural and dynamic information.[8] Due to their importance in nucleic acid investigations, novel fluorescent base analogues are being developed at a high pace, and many of them are used as probes for changes in their microenvironment.[9]

[a] *Dr. A. F. Füchtbauer, Dr. M. S. Wranne, S. Sarangamath, Prof. Dr. L. M. Wilhelmsson*
Department of Chemistry and Chemical Engineering
Chemistry and Biochemistry
Chalmers University of Technology
SE-412 96 Gothenburg (Sweden)
E-mail: marcus.wilhelmsson@chalmers.se
[b] *Dr. M. Bood, Prof. Dr. M. Grøtli*
Department of Chemistry and Molecular Biology
University of Gothenburg
SE-412 96 Gothenburg (Sweden)
[c] *Dr. A. H. El-Sagheer, Prof. Dr. T. Brown*
Department of Chemistry
University of Oxford
Chemistry Research Laboratory
12 Mansfield Road, Oxford, OX1 3TA (United Kingdom)
[d] *Dr. A. H. El-Sagheer*
Chemistry Branch
Department of Science and Mathematics
Faculty of Petroleum and Mining Engineering
Suez University
Suez, 43721 (Egypt)
[e] *Dr. M. Bood, Dr. H. Gradén*
Cardiovascular
Renal and Metabolic Diseases IMED Biotech Unit
AstraZeneca Gothenburg
Pepparedsleden 1
SE-431 83 Mölndal (Sweden)

Supporting information for this article is available on the WWW under https://doi.org/10.1002/cplu.201900712

Fb3 *This article is part of a Special Collection on "Fluorescent Biomolecules and their Building Blocks".*

Important recent developments include an isofunctional and isomorphic RNA alphabet,[10] a thymidine surrogate for site-specific Hg(II) binding in dsDNA,[11] and a tricyclic cytidine analogue with a turn-on response to duplex formation.[12]

In our group, we have developed and utilized a set of fluorescent tricyclic cytosine analogues, tC and tC^O, that maintain a high and virtually sequence-independent emission inside nucleic acids with minimal perturbation of the nucleic acid structure.[13] However, there has been a lack of fluorescent adenine analogues with the same valuable combination of properties. Starting from the excellent, but not so bright adenine analogue, quadracyclic adenine (qA),[14] we have recently developed adenine analogues that retain a significant brightness inside nucleic acids but with some sensitivity in quantum yield to their microenvironment, so far resulting in the bright and useful analogues qAN1 and pA.[15]

In a recent investigation of four promising adenine analogue monomers, qAN1-4 (qAN1 and qAN4 are shown in Figure 1), we found qAN4 to be even brighter than qAN1,[16] and hence, we decided to incorporate it into DNA to study its nucleobase analogue as well as photophysical properties. We here report the synthesis of the qAN4 phosphoramidite and its solid-phase incorporation into oligonucleotides, as well as its photophysical properties inside DNA. We show that qAN4 works very well as an adenine analogue, and exhibits useful micro-environment- and pH-sensitive emission properties. Furthermore, qAN4 forms an excellent base-analogue FRET-pair with the FRET acceptor qA_{nitro}.[15a] Thus, we here also contribute to expanding the currently limited library of nucleoside analogues that are well suited for interbase FRET and fluorescence anisotropy investigations.

Results and Discussion

In an effort to improve the brightness of the excellent adenine analogue qA,[14] we recently investigated a series of N^9-ethylated derivatives in this series of compounds, and found that monomeric qAN4 had the highest quantum yield (32%) and brightness ($\varepsilon\Phi_f = 2300\ M^{-1}cm^{-1}$) of the series, while retaining a large Stokes shift, making it a promising fluorescent adenine analogue.[16]

Here we have synthesized the phosphoramidite-protected quadracyclic 2′-deoxyadenosine analogue of qAN4 (**8**) over 9 steps in 18.9% overall yield from 9-((*tert*-butyldimethylsilyloxy) methyl)-6-chloro-7-(4,4,5,5-tetramethyl-1,3,2-dioxaborolan-2-yl)-7-deazapurine (**1**, Figure S1 in the Supporting Information), via a synthesis pathway analogous to that for qAN1 and pA (see Supporting Information for details).[15]

To establish the effect of replacing adenine with qAN4 on DNA structure and stability as well as to investigate the photophysical properties of qAN4 in various DNA environments, we incorporated qAN4 into 16 decamer sequences, in which qAN4 is flanked by all possible combinations of neighboring bases (Table 1). For details of the solid-phase oligonucleotide synthesis, see the Experimental Section.

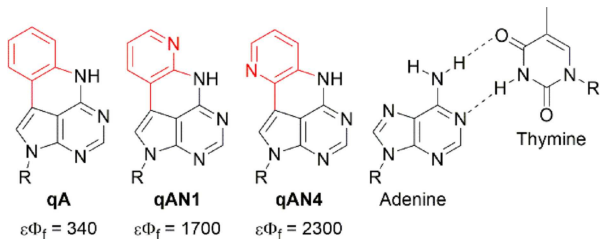

Figure 1. Structure of qA, qAN1, qAN4, and adenine base-paired with thymine, and their brightness values ($M^{-1}cm^{-1}$) as monomers.[14,16] Atoms of adenine (with N^7 replaced by C) and thymine are shown in black. R denotes the sugar-phosphate backbone.

Structure and stability of qAN4-modified duplexes

To investigate the effect of the incorporation of qAN4 on duplex stability, we measured the melting temperature of all 16 qAN4-modified duplexes and their unmodified counterparts (Table 1). Introducing qAN4 results in an average increase in duplex melting temperature of 5.6 °C – a greater change than that observed for qA (3.0 °C)[14] and qAN1 (2.9 °C).[15a] Overall, the stability increase is lowest when qAN4 is surrounded by two purines ($\Delta T_m = 2.5$ °C) and highest when qAN4 is surrounded by pyrimidines ($\Delta T_m = 8.7$ °C). This trend has also been observed for the parent compound qA and for qAN1, where it was attributed to the increase in base-stacking overlap that occurs between the extended quadracyclic ring system and a 5′-pyrimidine compared to a 5′-purine.[14–15] Moreover, the quadracyclic ring-system extends into the major groove of DNA, which rules out significant contributions to increased stacking compared to normal adenine between qAN4 and the nucleobases of the opposite strand. The increase in duplex stability

Table 1. Melting temperature of qAN4-containing duplexes (T_m^{qAN4}), unmodified duplexes (T_m^A), and the differences between them (ΔT_m).

Sample[a]	DNA sequence[b]	T_m^{qAN4} [°C][c]	T_m^A [°C][c]	ΔT_m [°C]
AA	5′-d(CGCA**AXA**TCG)-3′	44.3 ± 0.2	43.3 ± 0.2	1.0 ± 0.3
AC	5′-d(CGCA**AXC**TCG)-3′	51.2 ± 0.3	47.1 ± 0.2	4.1 ± 0.3
AG	5′-d(CGCA**AXG**TCG)-3′	49.0 ± 0.2	45.9 ± 0.2	3.1 ± 0.3
AT	5′-d(CGCA**AXT**TCG)-3′	48.2 ± 0.1	43.4 ± 0.1	4.8 ± 0.2
CA	5′-d(CGCA**CXA**TCG)-3′	53.1 ± 0.2	46.5 ± 0.1	6.6 ± 0.2
CC	5′-d(CGCA**CXC**TCG)-3′	59.5 ± 0.1	50.3 ± 0.1	9.2 ± 0.2
CG	5′-d(CGCA**CXG**TCG)-3′	56.8 ± 0.2	49.5 ± 0.1	7.3 ± 0.2
CT	5′-d(CGCA**CXT**TCG)-3′	56.2 ± 0.1	47.3 ± 0.1	8.9 ± 0.2
GA	5′-d(CGCA**GXA**TCG)-3′	47.0 ± 0.1	45.3 ± 0.2	1.7 ± 0.3
GC	5′-d(CGCA**GXC**TCG)-3′	54.5 ± 0.3	49.2 ± 0.2	5.3 ± 0.4
GG	5′-d(CGCA**GXG**TCG)-3′	52.4 ± 0.1	48.1 ± 0.2	4.3 ± 0.3
GT	5′-d(CGCA**GXT**TCG)-3′	50.7 ± 0.3	45.4 ± 0.2	5.3 ± 0.4
TA	5′-d(CGCA**TXA**TCG)-3′	45.5 ± 0.1	41.1 ± 0.3	4.4 ± 0.4
TC	5′-d(CGCA**TXC**TCG)-3′	52.1 ± 0.2	43.7 ± 0.1	8.4 ± 0.3
TG	5′-d(CGCA**TXG**TCG)-3′	50.4 ± 0.1	43.6 ± 0.1	6.8 ± 0.2
TT	5′-d(CGCA**TXT**TCG)-3′	49.0 ± 0.1	40.6 ± 0.1	8.4 ± 0.2

[a] All sequences are named by the bases neighboring qAN4 on the 5′- and 3′-side, respectively. [b] X = qAN4. In unmodified sequences, X = adenine. Duplexes were prepared by hybridization with their complementary sequence as described in the experimental section. [c] Samples were prepared in phosphate buffer, pH 7.5, 123 mM Na^+. The melting temperatures were determined using the maximum of the first derivative of the UV-melting curves. Measurements were duplicated and are reported with their standard errors.

that is observed upon incorporation of qAN4 is generally preferable over the reduced duplex stability observed for other purine FBAs such as 2-aminopurine (2-AP),[17] 3-MI,[18] 6MAP, DMAP[19] and xA.[20] Moreover, qAN4 offers a degree of tunability with respect to sequence surroundings in this regard (see Table 1), which could be a valuable property.

Base-pairing specificity

The base-pairing specificity of qAN4 was evaluated by the change in melting temperature upon annealing three sequences with sequences containing adenine, cytosine or guanine instead of thymine opposite qAN4 (Figure 2, Table S1). The chosen sequences have either two pyrimidines (CT), two purines (GA) or a mixture of both (TA) as neighboring bases to qAN4. In all cases, replacing T with either G, C or A has a significant destabilizing effect on DNA stability, which strongly suggests that qAN4 specifically base-pairs with thymine. The smallest decrease in melting temperature was observed for guanine mismatches (average 11.8 °C), whereas A- and C-mismatches resulted in an average decrease of 17.1 and 17.2 °C, respectively. The same trend was previously found for the parent molecule qA.[14] Some base analogues, including 2-AP, have been shown to base-pair with several bases and to decrease the thermal stability of DNA.[21] Only a handful of FBAs like thA,[22] ^{tz}A,[10b] qA,[14] qAN1[15a] and pA[15b] have been shown to offer such specificity towards complementary bases. The finding that qAN4 base-pairs specifically with T is an important quality for its possible use as a fluorescent adenine base analogue.

Circular Dichroism (CD)

To investigate the effect of incorporation of qAN4 on the secondary structure of DNA, CD was measured on all 16 qAN4-modified duplexes and the corresponding unmodified DNA-duplexes. The usual characteristics for a B-form DNA duplex are found in all the CD spectra (Figure S2 and S3): a positive band between 260 and 280 nm, a negative band around 250 nm and a sharp positive peak around 200 nm.[23] There are minor variations between CD-spectra of the modified and unmodified duplexes, most likely due to differences in the absorption spectrum of qAN4 compared to the adenine that is replaced. As for the parent compound, qA, the long-wavelength absorption band for qAN4 is not observed in any of the CD spectra.[14]

Taken together, the structural characterization using CD, thermal melting and mismatch data all suggest that qAN4 is an excellent adenine analogue that does not significantly alter the DNA structure and that base-pairs specifically with thymine.

Spectroscopic characterization of qAN4 inside DNA

Figure 3 shows representative absorption and emission spectra of the qAN4-monomer and in single- and double-stranded DNA (ssDNA and dsDNA; see Figure S4 for all absorption spectra and Figure S5 for all emission spectra). The absorption maxima for qAN4 (356 nm as a monomer) is essentially unchanged when incorporated into DNA (~358 nm for both ss- and dsDNA), and, similarly to other nucleobase analogues, lies well outside the absorption of natural nucleobases.[5] Thus, it can be selectively excited when qAN4 is incorporated into DNA.

The emission intensity of qAN4 once incorporated into ssDNA is sensitive to the nature of its neighboring bases (Table 2; see Figure S5 for emission spectra), whereas the emission maximum is reasonably unchanged in ssDNA (Figure 3, 414–424 nm). Compared to free qAN4 in solution ($\lambda_{em,max}$ = 456 nm) there is a substantial blue-shift of 32–42 nm (1700–2200 cm^{-1}) of emission of qAN4 in ssDNA. This blue-shift is most likely an effect of the more hydrophobic environment surrounding qAN4 inside ssDNA compared to water. This increases the energy gap between the less polar ground-state and the more polar excited state giving rise to emission at shorter wavelengths.

The fact that different neighboring bases give variation in fluorescence intensities (Table 2) implies that the emission of qAN4 is environment responsive and, thus, can be used for

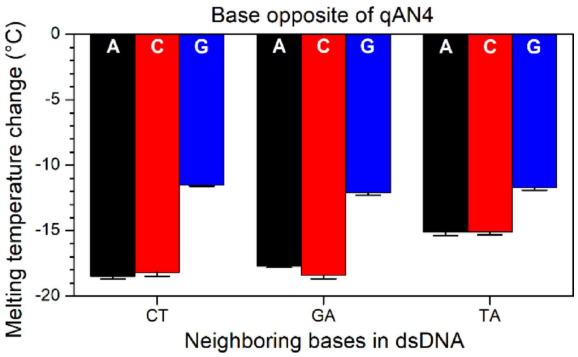

Figure 2. The difference in T_m between mismatched (A, C, or G opposite qAN4) and the corresponding matched sequences (T opposite qAN4) for three sets of nearest neighbors to qAN4 (CT, GA, and TA).

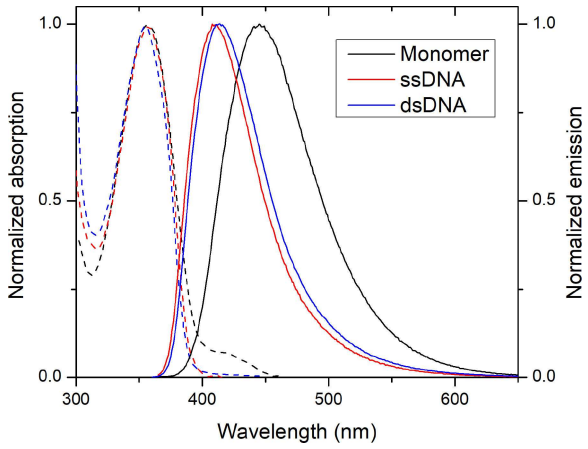

Figure 3. Normalized absorption (dashed lines) and emission (solid lines, λ_{ex} = 356 nm) spectra of qAN4 as a monomer, in ssDNA (sequence AA; see Table 1 for sequence names) and in dsDNA (duplex AA). Measurements were performed at RT in phosphate buffer, pH 7.5, 123 mM Na^+.

Table 2. Quantum yields and average fluorescence lifetimes of single- and double-stranded DNA containing qAN4.[a]

Sample[b]	Single-stranded DNA				Double-stranded DNA			
	Φ_f [%][c]	$<\tau>$ [ns][d]	k_r [10^7 s^{-1}][e]	k_{nr} [10^8 s^{-1}][f]	Φ_f [%][c]	$<\tau>$ [ns][d]	k_r [10^7 s^{-1}][e]	k_{nr} [10^8 s^{-1}][f]
AA	29.4 ± 0.3	5.90	5.0	1.2	7.1 ± 0.2	1.73	4.1	5.4
AC	5.0 ± 0.3	0.95	5.2	10.0	1.4 ± 0.1	0.36	3.8	27.3
AG	15.9 ± 0.4	3.03	5.2	2.8	5.7 ± 0.1	1.49	3.9	6.4
AT	3.7 ± 0.1	0.89	4.1	10.8	3.3 ± 0.1	1.14	3.1	9.2
CA	6.9 ± 0.2	1.22	5.6	7.6	2.4 ± 0.1	0.60	4.0	16.4
CC	1.5 ± 0.1	0.31	5.0	31.7	0.90 ± 0.03	0.25	3.9	43.0
CG	2.3 ± 0.1	0.44	5.3	22.0	1.8 ± 0.1	0.48	3.8	21.0
CT	1.2 ± 0.1	0.24	5.0	40.9	1.5 ± 0.1	0.52	3.1	19.5
GA	20.9 ± 0.3	4.55	4.6	1.7	3.7 ± 0.2	0.96	3.8	10.0
GC	3.7 ± 0.1	0.73	5.1	13.1	0.78 ± 0.02	0.22	3.5	44.6
GG	15.2 ± 0.3	3.33	4.6	2.5	3.5 ± 0.2	0.95	3.7	10.2
GT	2.6 ± 0.1	0.64	4.0	15.2	1.3 ± 0.1	0.49	2.6	20.3
TA	4.9 ± 0.2	0.73	6.7	13.0	1.9 ± 0.1	0.55	3.3	17.7
TC	1.2 ± 0.1	0.32	3.8	31.1	1.2 ± 0.1	0.37	3.2	26.4
TG	1.9 ± 0.1	0.35	5.3	27.8	1.4 ± 0.1	0.43	3.3	22.8
TT	0.95 ± 0.02	0.22	4.3	45.2	2.3 ± 0.1	0.77	3.0	12.7

[a] Measurements were performed at 4 μM concentration in phosphate buffer (pH 7.5, 123 mM Na^+) at RT. [b] Sequences were named according to the bases neighboring qAN4; full sequences can be found in Table 1. [c] Quantum yields were determined using the emission profiles shown in Figure S5, with quinine sulphate in 0.5 M H_2SO_4 as a reference ($\Phi_f = 54.6\%$), using an excitation wavelength of 356 nm. Measurements were duplicated and are reported with their standard error. [d] Fluorescence decays were measured using a TCSPC setup with a laser diode emitting at 377 nm and emission collection at 415 nm. For details see Table S2 and Table S3. [e] Radiative rate constant, $k_r = \Phi_f / <\tau>$. [f] Non-radiative rate constant, $k_{nr} = k_r/\Phi_f - k_r$.

applications similar to 2-AP and other environment-responsive nucleic acid probes.[4,7a,9b] The quantum yield of qAN4 inside ssDNA is quenched compared to the free monomer in water ($\Phi_f = 32\%$). Even the most emissive strand (AA; $\Phi_f = 29.4\%$, see Table 2), exhibits a decrease in quantum yield when going from monomer to single strand. As can be seen in Table 2, the quenching is smallest when the neighboring bases are both purines and largest when the neighboring bases are both pyrimidines. The most quenched ssDNA (TT) has a quantum yield of 0.95%, more than 30 times lower than the least quenched single strand (AA). The average quantum yield of qAN4 modified ssDNA is 7.3%, resulting in an average brightness ($\varepsilon \times \Phi_f$) of 800 $M^{-1}cm^{-1}$. The quantum yield in single strands is 3.9 times higher than that quantum yield of its parent compound, qA (1.9%),[14] and similar to the recently reported qAN1 (6.3%).[15a]

In DNA duplexes, the emission of qAN4 is also sensitive to the nature of its neighboring bases (Figure S5). The position of the emission maximum (406–414 nm) for qAN4 in duplex DNA is slightly blue-shifted compared to the single-stranded case (*vide supra*).

The quantum yield of qAN4 is generally quenched further when going from ss- to dsDNA (Table 2). However if qAN4 is neighboring a thymine, the quenching is reduced compared to the single-stranded case. As in single-strands, qAN4 has the highest quantum yield in the AA-sequence ($\Phi_f = 7.1\%$), and neighboring purines have a smaller quenching effect than pyrimidines (Table 2). The average brightness of qAN4 in double-stranded DNA is 275 $M^{-1}cm^{-1}$, which is more than 5-fold higher than the most used environment-sensitive fluorescent base analogue, 2-AP[21] and 15-fold brighter than the parent compound, qA,[14] but about half as bright as the recently reported qAN1 (510 $M^{-1}cm^{-1}$).[15a]

A striking and interesting feature, which has also been found for other members of the qA-family and the tricyclic cytosines, is that neighboring guanines do not result in a quenched emission compared to most other neighboring base-combinations; in the qA-family, they are rather among the least quenched ones.[14–15] Generally, adjacent guanine quenches the quantum yield of a large number of known fluorescent nucleobase analogues by photo-induced electron transfer (PET) because of guanine's low redox potential compared to the other natural nucleobases. However, like other members of the qA-family, guanine has a smaller quenching effect on qAN4 that is more similar to the effect of adenine than to the pyrimidines. We suggest that this counterintuitive trend in guanine quenching of qAN4 is instead an effect of the base analogue donating electrons to the surrounding bases. The higher quenching in pyrimidine surroundings could then be explained by their higher propensity to accept electrons from qAN4 compared to the purines, including guanine. We observe similar trends in quantum yield depending on surrounding bases for qA, qAN1 and qAN4.[14–15] However, there are slight differences and more importantly, the amount of fluorescence quenching differs. This may be explained by the position or lack of nitrogen in the other ring of the qA-derivatives. For example, since the nitrogen of qAN4 is facing outwards from the base-stack compared to the nitrogen of qAN1 that faces the hydrogen bonding region of the base-pair it is more solvated by water and, thus, is in a more hydrophilic and polar environment. Such variations would certainly affect the photophysics and quenching pathways for these three quadracyclic adenine analogues. The intrinsic effect of the changes of the outer ring of the qA-derivatives on the electronic states of the molecules is another plausible explanation for the variations we find.

The average lifetimes for qAN4 in ssDNA vary between 0.22 and 5.90 ns, whereas those for qAN4 in duplexes vary between

0.22 and 1.71 ns (see Table 2). For all qAN4-modified sequences, a decrease in quantum yield is, as expected, accompanied by a shortening of the fluorescence lifetime. The emission decay curves mostly had to be fitted to tri-exponential expressions for the samples (for details see Supporting information, Table S2 and S3). This is similar to the corresponding data for qAN1 and pA,[15] whereas fewer lifetimes were needed to fit the tricyclic cytosine family.[13a,c]

The calculated radiative and non-radiative rate constants for qAN4 in ssDNA range between 3.8 and $6.7\times10^{7}\ s^{-1}$ and between 1.2 and $45.2\times10^{8}\ s^{-1}$, respectively. The radiative rate constant remains largely unchanged across the series, and the varying degree of quenching observed across the series is therefore due to non-radiative quenching pathways, most likely originating from differences in stacking interactions and the electron transfer processes mentioned above – with pyrimidines generally providing the strongest quenching effect. The same trend can be observed in dsDNA, albeit with a slightly smaller fluctuation in the non-radiative rate constants ($5.4–44.6\times10^{8}\ s^{-1}$).

pH sensitivity of qAN4 in dsDNA

When studying the qAN4-modified DNA, we found the qAN4 absorption spectra to be pH-dependent with a weak band above 400 nm appearing in acidic conditions. To examine whether this is due to a protonation effect, absorption and emission spectra of four qAN4-modified duplexes (CC, GG, AT, TA) were measured at pH 5 (Figure 4). At pH 7.5, the absorption spectra of all four duplexes have a weak shoulder above 400 nm, along with the expected absorption band centered at 356 nm. At pH 5 this band increases to become more significant in the absorption spectra of all four duplexes. In quantum chemical calculations we also find significant red-shifts of the lowest energy transition compared to qAN4 when protonating position 4 of the outer ring of qAN4 or position 1 of the adenine ring system (111 and 49 nm, respectively, compared to corresponding values for unprotonated qAN4). In our absorption measurements the peak for the protonated species seem to be shifted by approximately 70 nm compared to the lowest transition of the qAN4 absorption (Figure 4), which suggests that protonation is a plausible explanation of the red-shift of qAN4 at low pH.

In the emission spectrum of these four duplexes at pH 5, an emission band centered slightly below 500 nm appears (Figure 5). This is most obvious for the AT- and TA-sequences but can also be seen as a slight increase in the band intensity above 450 nm for CC and GG. The overall emission of AT is quenched significantly at pH 5 compared to at pH 7.5, whereas the opposite is true for the TA sequence. To examine whether the shoulder peak for the AT and TA duplexes originates from the long-wavelength absorption band species, emission spectra of the AT- and TA-duplexes were measured at an excitation wavelength of 415 nm (Figure 5, right). The emission spectra clearly show only one major band centered at 480–500 nm which overlaps well with the corresponding shoulder in emission spectra which was excited at 356 nm (solid lines in Figure 5). This dependency shows that qAN4 can be used as a pH-sensitive probe inside nucleic acids when flanked by certain neighboring sequences.

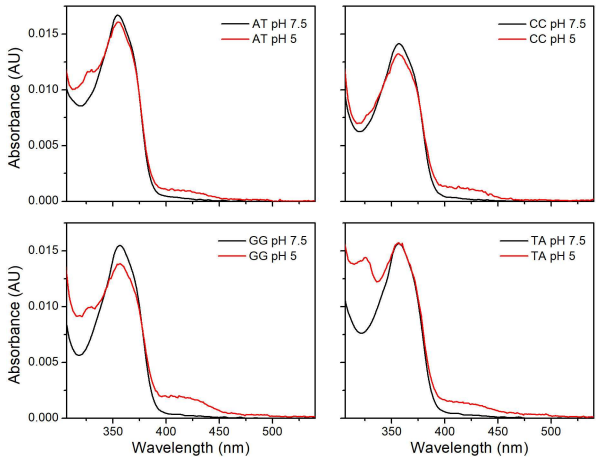

Figure 4. Absorption spectra of qAN4-modified duplexes (AT, TA, CC and GG) at pH 5 and pH 7.5. Measurements were performed at RT in phosphate buffer (pH 5: citrate-phosphate buffer with 12.5 mM phosphate and 123 mM Na^{+}; pH 7.5: 12.5 mM phosphate and 123 mM Na^{+}).

FRET between qAN4-qA_{nitro} in DNA

To evaluate the potential of qAN4 as a FRET donor, the normalized emission of qAN4 and the absorption of qA_{nitro} were overlaid (Figure 6). There is a significant overlap between this donor-acceptor pair, giving a Förster radius, R_0, of 25 Å using the orientation factor, $\kappa^2=2/3$ for the highest quantum yield duplex. This would enable the study of distances which are almost 1.5 turns of the B-DNA helix.[13d] The used κ^2 value is for freely rotating fluorophores and has been used for comparison only. However, the actual orientation factor for firmly stacked probes inside DNA changes depending on the separation between the donor and the acceptor since there is a helical twist of 34.3 degrees with each increase in the number of bases separating the donor and acceptor. To determine the effect of

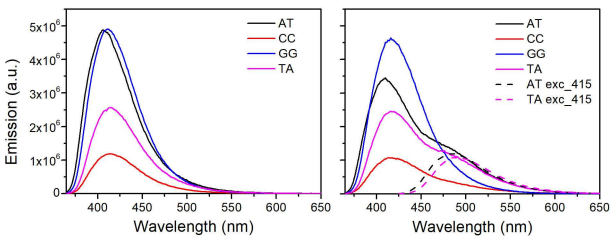

Figure 5. Emission spectra of qAN4-modified duplexes (AT, TA, CC and GG) at pH 7.5 (left) and pH 5 (right). The excitation spectra of AT and TA ($\lambda_{exc}=415$ nm) at pH 5 is also shown in the graph to the right. Measurements were performed at RT in phosphate buffer (pH 5: citrate-phosphate buffer with 12.5 mM phosphate and 123 mM Na^{+}; pH 7.5: 12.5 mM phosphate and 123 mM Na^{+}).

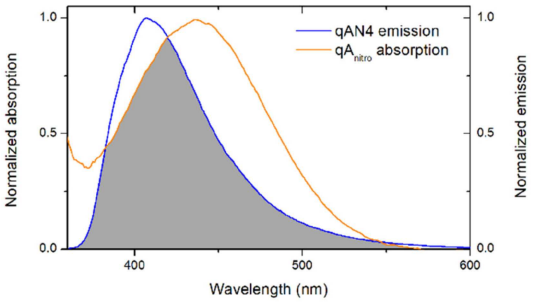

Figure 6. Spectral overlap between qAN4 emission and qA$_{nitro}$ absorption in dsDNA. Spectra are normalized at their wavelength maxima. qAN4 dsDNA was excited at 356 nm and the measurements were performed at RT in phosphate buffer (pH 7.5, 123 mM Na^+).

Table 3. List of 33-mer DNAs used in the FRET study.

Sequence name[a]	DNA sequence[b]	Φ_f [%][c]
D7	5′-d(CGA TCA **(qAN4)**AA AAA ATT X)-3′	5.9 ± 0.1
D9	5′-d(CGA TCA AA**(qAN4)** AAA ATT X)-3′	6.9 ± 0.1
D11	5′-d(CGA TCA AAA A**(qAN4)**A ATT X)-3′	8.0 ± 0.2
A13	5′-d(Y TAT **(qA$_{nitro}$)**AT CGT AAT Z)-3′	
A14	5′-d(Y TAT A**(qA$_{nitro}$)**T CGT AAT Z)-3′	
A19	5′-d(Y TAT AAT CGT **(qA$_{nitro}$)**AT Z)-3′	
A20	5′-d(Y TAT AAT CGT A**(qA$_{nitro}$)**T Z)-3′	
A0	5′-d(Y TAT AAT CGT AAT Z)-3′	

[a] Sequences are named by the donor (D) or acceptor (A) position from the 5′ end. [b] X = ACG ATT ATA AGG AGG AGG, Y = CCT CCT CCT and Z = TTT TTT TGA TCG. [c] Quantum yields are determined with quinine sulfate as reference (Φ_f = 54.6% in 0.5 M H_2SO_4) with an excitation wavelength of 356 nm. Measurements were duplicated and are reported with their standard error. Samples were prepared as described in the experimental section and measured at RT in phosphate buffer (pH 7.5, 123 mM Na^+).

distance and orientation on the FRET-efficiency, three donor strands, four acceptor strands and an unmodified strand, each 33 bases long, were prepared (Table 3). These were designed in such a way that the distance between the donor and the acceptor in duplexes could be varied from 2 to 13 base pairs. The quantum yields of dsDNA containing only the donor (qAN4) were measured for the subsequent evaluation of the FRET data and found to be slightly increasing as qAN4 is moved away from the 5′ end (Table 3). A similar trend was observed for both qAN1 and pA and has been hypothesized to be due to slight changes in the local environment.[15]

The FRET efficiencies of all 12 duplexes were measured as a change in the steady-state emission and average fluorescence lifetime of qAN4. Figure 7 contains the FRET efficiencies between qAN4 and qA$_{nitro}$ as a function of the number of base pairs separating the two. Initially, when the distance between the donor and acceptor is short, the FRET efficiency is high. It starts to decrease significantly at a base-pair separation of 5 and then fluctuates between local maxima and minima as expected for firmly stacked FBA FRET-pairs inside dsDNA. This pattern has also been found for the tC°-tC$_{nitro}$, qAN1-qA$_{nitro}$ and pA-qA$_{nitro}$ FRET pairs[13d,15] and can be explained by the change in orientation between the donor and the acceptor in dsDNA as the separation increases between them and the helicity of the B-form DNA changes their relative orientation. To fit a theoretical curve to the measured data, an in-house developed MATLAB code was used (for details of the FRET-theory and the fitting procedure see the Supporting Information). The best fit is obtained for an overlap integral of 1.92×10^{14} $nm^4\,cm^{-1}\,M^{-1}$ and a phase angle of 42 degrees (the angle between the donor and acceptor transition dipole moments at zero base-pair separation). To compare this, the overlap integral for the qAN4 and qA$_{nitro}$ spectral profiles were calculated to be 1.3×10^{14} $nm^4\,cm^{-1}\,M^{-1}$ which is close to the fitted value.

Using time-dependent density functional theory (TDDFT)-calculations, the orientation of the transition dipole moments of qAN4 and qA$_{nitro}$ has been predicted, and the associated phase angle is 25 degrees (see SI for details of the TDDFT calculation).[13d,15a] The difference between this theoretical value and the one estimated above using FRET may be an effect of slight discrepancies between the theoretical and the actual

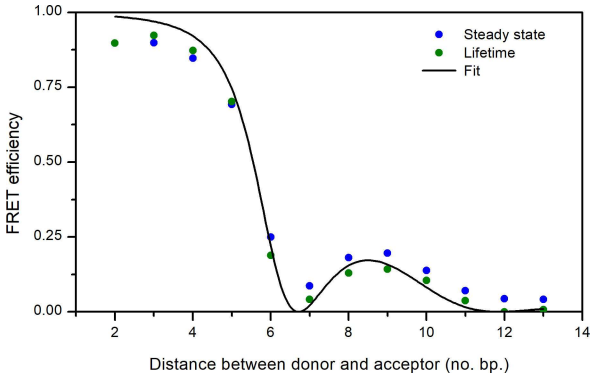

Figure 7. FRET efficiency as a function of base-pair separation between qAN4 (donor) and qA$_{nitro}$ (acceptor). Blue and green circles denote data from steady-state and lifetime measurements, respectively. The line denotes the curve fitted to the data based on FRET-theory as mentioned in the Supporting Information. Measurements were performed at RT in phosphate buffer at pH 7.5 and 123 mM Na^+.

direction of the transition dipole moments of the two molecules comprising the FRET-pair as well as limitations in the model we use to fit the FRET-data (for example, the model disregards dynamics and merely uses an average B-form DNA not taking into account any sequence information). The orientation and distance-dependent FRET behavior for our new probe pair makes qAN4-qA$_{nitro}$ a useful addition to the limited number of FBA FRET-pairs that are available so far. Due to its spectral properties, qAN4, like qAN1, could also be combined with tC$_{nitro}$ as an acceptor.

Conclusion

We present here a fluorescent adenine analogue, qAN4, which is more than one order of magnitude brighter than the parent compound, qA. Moreover, we show in mismatch studies that qAN4 is an excellent and specific adenine analogue. Combining these two features makes qAN4 a promising fluorescent base analogue. We also find the photophysical properties of qAN4 to

be sensitive towards its flanking bases and pH, the latter suggesting future possible applications in biology for probing the pH of the local environment of the nucleic acid. Its emissive properties overlap well with the absorption of qA_{nitro} and enable accurate FRET-measurements over more than one turn of B-DNA. Furthermore, qAN4 can act as a donor to the previously developed C-analogue acceptor, tC_{nitro}, to constitute an A to C interbase FRET-pair. The quadracyclic adenine family continues to provide excellent analogues of adenine with a range of useful properties and investigations regarding new derivatives of this family are ongoing.

Experimental Section

Synthesis

All reactions were performed in flame-dried or oven-dried glassware under a nitrogen atmosphere unless otherwise noted. Reagents were purchased from various chemical vendors and either used as received or purified according to standard techniques. All solvents used for reactions were purchased dry. Microwave reactions were performed with a Biotage Initiator using single-mode microwave irradiation with temperature and pressure control and with fixed hold time on. Reactions were monitored by TLC on silica gel plates analyzed under UV (254 nm), and by UPLC-MS (ESI/UV), using a Waters Acquity system equipped with either an Acquity UPLC HSS C18 column (1.8 μm, length 50 mm, ID 2.1 mm) running a gradient of water-MeCN (95:5) to water-MeCN (5:95), with the water eluent containing 1% formic acid (pH 3) or an Acquity UPLC BEH C18 column (1.7 μm, length 50 mm, ID 2.1 mm) running a gradient of water-MeCN (95:5) to water-MeCN (5:95), with the water eluent containing 1% ammonium hydroxide (pH 10). Flash chromatography was performed by automated column chromatography using pre-packed silica columns. HPLC purification was performed with ammonia as modifier on a preparative HPLC system with an Xbridge C18 column (10 μm, 250×50 mm). ^{1}H and ^{13}C NMR spectra were recorded on a Bruker 500 MHz system equipped with a CryoProbe. All shifts are recorded in ppm relative to the deuterated solvent: $CDCl_3$ (7.26 ppm for ^{1}H and 77.16 ppm for ^{13}C) or DMSO-d_6 (2.50 ppm for ^{1}H and 39.52 ppm for ^{13}C). 2D-NMR spectra (COSY, HSQC and HMBC) were used for peak assignments and detection of peaks overlapping with the deuterated solvent.

Oligonucleotide synthesis and purification

Oligonucleotide synthesis was carried out on an Applied Biosystems 394 automated DNA/RNA synthesizer using a standard 1.0 μmole phosphoramidite cycle of acid-catalyzed detritylation, coupling, capping and iodine oxidation. All β-cyanoethyl phosphoramidite monomers were dissolved in anhydrous acetonitrile to a concentration of 0.1 M immediately prior to use. The coupling time for normal A, G, C, and T monomers was 60 s and this was extended to 900 s for the qAN4 monomer. Stepwise coupling efficiencies and overall yields were determined by automated trityl cation conductivity monitoring and in all cases were >98.0%. Cleavage of oligonucleotides from the solid support and deprotection were achieved by exposure to concentrated aqueous ammonia for 60 min at room temperature followed by heating in a sealed tube for 5 h at 55 °C. Purification of oligonucleotides was carried out by reversed-phase HPLC on a Gilson system using a Brownlee Aquapore column (C8, 8 mm×250 mm, 300 Å pore) with a gradient of acetonitrile in triethylammonium bicarbonate (TEAB) increasing from 0% to 50% buffer B over 30 min with a flow rate of 4 mL/min (buffer A: 0.1 M triethylammonium bicarbonate, pH 7.0, buffer B: 0.1 M triethylammonium bicarbonate, pH 7.0 with 50% acetonitrile). The elution of oligonucleotides was monitored by ultraviolet absorption at 295 or 300 nm. After HPLC purification, oligonucleotides were freeze-dried then dissolved in water without the need for desalting. All oligonucleotides were characterized by electrospray mass spectrometry using a Bruker micrOTOF II focus ESI-TOF MS instrument in ESI- mode. Data were processed using MaxEnt.

Sample preparation

Unless stated otherwise, a 12.5 mM phosphate buffer of pH 7.5 with a total sodium ion concentration of 123 mM was used. For pH 5 samples a 12.5 mM citrate buffer at pH 5 with a total sodium ion concentration of 123 mM was used. Concentration determinations of single-stranded samples and measurement of absorption spectra were performed using a Cary 5000 UV-Vis absorption spectrophotometer (Varian Technologies). All measurements were blank corrected. To afford the DNA duplexes used in the emission measurements, 4 or 8 μM of modified ssDNA were mixed with 4.6 or 9.2 μM of their complementary (unmodified) single strands to arrive at a final concentration of duplexes of 2 or 4 μM. The excess of complementary strands was prepared to ensure that all the modified strands were incorporated in a duplex and, thus, to avoid fluorescence signal from any unhybridized, modified single strand. The unmodified duplexes used for melting and CD-analysis were prepared in a similar manner. The samples were annealed by heating to 90 °C for 5 minutes, followed by slow cooling to 5 °C overnight. The molar absorptivity of the sequences was calculated by the summation of the molar absorptivities of the individual natural bases and qAN4. This sum was multiplied by 0.9 to correct for base stacking interactions. The extinction coefficient at 260 nm of qAN4 in water was determined to be 6600 $M^{-1}cm^{-1}$ by measuring the absorption of a solution with a known concentration of qAN4. The extinction coefficients that were used for the different bases at 260 nm were $\varepsilon_T = 9300\ M^{-1}cm^{-1}$, $\varepsilon_C = 7400\ M^{-1}cm^{-1}$, $\varepsilon_G = 11800\ M^{-1}cm^{-1}$, $\varepsilon_A = 15300\ M^{-1}cm^{-11}$. Molar absorptivities of the unmodified oligonucleotides were calculated in the same way.

Fluorescence measurements

Steady-state fluorescence measurements were performed on a SPEX Fluorolog 3 spectrofluorimeter (JY Horiba). Samples were excited at the lowest energy absorption maximum for qAN4, 356 nm. The emission was recorded between 360 and 700 nm and all readings were blank corrected and corrected for the wavelength dependence of the optics and detectors. The measurements were done in duplicate with the excitation and emission slit widths kept at 1.3 and 2.8 nm, respectively. Quinine sulphate in 0.5 M H_2SO_4 was used as the quantum yield reference ($\Phi_f = 0.546$).

Fluorescence lifetimes of modified DNA samples were each measured once using time-correlated single-photon counting (TCSPC). Samples were excited by a Picoquant pulsed (10 MHz) laser diode emitting at 377 nm. The emission monochromator was set to 415 nm. The counts were collected by an R3809 U-50 microchannel-plate photomultiplier tube (Hamamatsu) and fed into a Lifespec multi-channel analyzer (Edinburgh Analytical instruments) with 2048 channels. 10000 counts were recorded in the top channel. Reconvolutional fitting was performed using Fluofit Pro V.4 software (PicoQuant GmbH). The average lifetimes were amplitude weighted according to Equation (1):

$$\langle\tau\rangle = \frac{\sum_{i-1}^{j} a^i \tau^i}{\sum_{i-1}^{j} a^i} \quad (1)$$

Where $<\tau>$ is the average lifetime, α^i is the i^{th} lifetime and τ^i is the amplitude of the i^{th} lifetime.

UV melting experiments

Thermal melting curves were recorded on a Cary 4000 (Varian technologies) with a programmable multi-cell temperature block, by heating from 15 to 80 °C at a rate of 0.5 °C/min followed by cooling to 15 °C at a rate of 0.5 °C/min. The absorption at 260 nm was recorded at every 0.5 °C. The maximum of the UV melting first derivative curve was used to determine the melting temperature of the DNA strands. The concentration of duplexes was 2 μM. Measurements were duplicated.

Circular dichroism (CD)

CD spectra were recorded on a Chirascan CD spectrometer (Applied Photophysics) at 20 °C, scanning between 200–450 nm, at a scan rate of 1 nm/s, using an integration time of 0.5 s and four repetitions. All spectra were blank corrected and smoothed (5-point Salvitzky-Golay). The concentration of duplexes was kept at 2 μM.

FRET measurements

Using the eight sequences listed in Table 3, 15 different duplexes were hybridized, three with only the donor qAN4 present (at three different positions) and 12 with the donor qAN4 in one strand and the acceptor qA_{nitro} in the opposite strand, resulting in duplexes with 2–13 bases separating the donor and acceptor. Hybridization was performed as described above, using 30% excess of the unmodified or acceptor strands compared to those containing the donor qAN4. Steady-state emission spectra (on SPEX Fluorolog 3) and time-resolved decays (TCSPC) were measured for all samples using the same settings as described above. The duplex concentration was 4 μM in all measurements. Quantum yields were measured on the three duplexes with only qAN4 present (*i.e.* no qA_{nitro}) as described above. Measurements were duplicated.

Acknowledgements

This work was supported by the Swedish Foundation for Strategic Research (SSF, grant No. IS14-0041) and the Swedish Research Council (VR, grant No. 2017-03707).

Keywords: base pairing · DNA · FRET · nucleobase analogues · photophysics

[1] M. P. Foster, C. A. McElroy, C. D. Amero, *Biochemistry* **2007**, *46*, 331–340.
[2] S. R. Holbrook, *Annu. Rev. Biophys.* **2008**, *37*, 445–464.
[3] W. Kühlbrandt, *eLife* **2014**, *3*, e03678.
[4] L. M. Wilhelmsson, Y. Tor, *Fluorescent Analogs of Biomolecular Building Blocks: Design and Applications*, John Wiley & Sons, **2016**.
[5] D. Onidas, D. Markovitsi, S. Marguet, A. Sharonov, T. Gustavsson, *J. Phys. Chem. B* **2002**, *106*, 11367–11374.
[6] J. N. Wilson, E. T. Kool, *Org. Biomol. Chem.* **2006**, *4*, 4265–4274.
[7] a) W. Xu, K. M. Chan, E. T. Kool, *Nat. Chem.* **2017**, *9*, 1043–1055; b) M. Bood, S. Sarangamath, M. S. Wranne, M. Grøtli, L. M. Wilhelmsson, *Beilstein J. Org. Chem.* **2018**, *14*, 114–129.
[8] a) A. Iqbal, S. Arslan, B. Okumus, T. J. Wilson, G. Giraud, D. G. Norman, T. Ha, D. M. Lilley, *Proc. Natl. Acad. Sci. USA* **2008**, *105*, 11176–11181; b) F. D. Lewis, L. G. Zhang, X. B. Zuo, *J. Am. Chem. Soc.* **2005**, *127*, 10002–10003; c) S. Preus, L. M. Wilhelmsson, *ChemBioChem* **2012**, *13*, 1990–2001; d) S. Kalinin, T. Peulen, S. Sindbert, P. J. Rothwell, S. Berger, T. Restle, R. S. Goody, H. Gohlke, C. A. M. Seidel, *Nat. Methods* **2012**, *9*, 1218–1225; e) I. König, A. Zarrine-Afsar, M. Aznauryan, A. Soranno, B. Wunderlich, F. Dingfelder, J. C. Stüber, A. Plückthun, D. Nettels, B. Schuler, *Nat. Methods* **2015**, *12*, 773–779; f) M. Sustarsic, A. N. Kapanidis, *Curr. Opin. Struct. Biol.* **2015**, *34*, 52–59; g) J. R. Lakowicz, *Principles of fluorescence spectroscopy*, 2nd ed., Springer, New York, **2006**.
[9] a) D. W. Dodd, R. H. E. Hudson, *Mini-Rev. Org. Chem.* **2009**, *6*, 378–391; b) R. W. Sinkeldam, N. J. Greco, Y. Tor, *Chem. Rev.* **2010**, *110*, 2579–2619; c) L. M. Wilhelmsson, *Q. Rev. Biophys.* **2010**, *43*, 159–183; d) N. B. Gaied, N. Glasser, N. Ramalanjaona, H. Beltz, P. Wolff, R. Marquet, A. Burger, Y. Mély, *Nucleic Acids Res.* **2005**, *33*, 1031–1039.
[10] a) D. Shin, R. W. Sinkeldam, Y. Tor, *J. Am. Chem. Soc.* **2011**, *133*, 14912–14915; b) A. R. Rovira, A. Fin, Y. Tor, *J. Am. Chem. Soc.* **2015**, *137*, 14602–14605.
[11] G. Mata, O. P. Schmidt, N. W. Luedtke, *Chem. Commun.* **2016**, *52*, 4718–4721.
[12] D. D. Burns, K. L. Teppang, R. W. Lee, M. E. Lokensgard, B. W. Purse, *J. Am. Chem. Soc.* **2017**, *139*, 1372–1375.
[13] a) L. M. Wilhelmsson, P. Sandin, A. Holmen, B. Albinsson, P. Lincoln, B. Norden, *J. Phys. Chem. B* **2003**, *107*, 9094–9101; b) K. C. Engman, P. Sandin, S. Osborne, T. Brown, M. Billeter, P. Lincoln, B. Nordén, B. Albinsson, L. M. Wilhelmsson, *Nucleic Acids Res.* **2004**, *32*, 5087–5095; c) P. Sandin, K. Börjesson, H. Li, J. Mårtensson, T. Brown, L. M. Wilhelmsson, B. Albinsson, *Nucleic Acids Res.* **2008**, *36*, 157–167; d) K. Börjesson, S. Preus, A. H. El-Sagheer, T. Brown, B. Albinsson, L. M. Wilhelmsson, *J. Am. Chem. Soc.* **2009**, *131*, 4288–4293.
[14] A. Dierckx, F. A. Miannay, N. Ben Gaied, S. Preus, M. Björck, T. Brown, L. M. Wilhelmsson, *Chem. Eur. J.* **2012**, *18*, 5987–5997.
[15] a) M. S. Wranne, A. F. Füchtbauer, B. Dumat, M. Bood, A. H. El-Sagheer, T. Brown, H. Gradén, M. Grøtli, L. M. Wilhelmsson, *J. Am. Chem. Soc.* **2017**, *139*, 9271–9280; b) M. Bood, A. F. Füchtbauer, M. S. Wranne, J. J. Ro, S. Sarangamath, A. H. El-Sagheer, D. L. M. Rupert, R. S. Fisher, S. W. Magennis, A. C. Jones, F. Höök, T. Brown, B. H. Kim, A. Dahlén, L. M. Wilhelmsson, M. Grøtli, *Chem. Sci.* **2018**, *9*, 3494–3502.
[16] B. Dumat, M. Bood, M. S. Wranne, C. P. Lawson, A. F. Larsen, S. Preus, J. Streling, H. Gradén, E. Wellner, M. Grøtli, L. M. Wilhelmsson, *Chem. Eur. J.* **2015**, *21*, 4039–4048.
[17] D. Xu, K. O. Evans, T. M. Nordlund, *Biochemistry* **1994**, *33*, 9592–9599.
[18] M. E. Hawkins, W. Pfleiderer, F. M. Balis, D. Porter, J. R. Knutson, *Anal. Biochem.* **1997**, *244*, 86–95.
[19] M. E. Hawkins, *Cell Biochem. Biophys.* **2001**, *34*, 257–281.
[20] J. Gao, H. Liu, E. T. Kool, *J. Am. Chem. Soc.* **2004**, *126*, 11826–11831.
[21] A. C. Jones, R. K. Neely, *Q. Rev. Biophys.* **2015**, *48*, 244–279.
[22] R. A. Mizrahi, D. Shin, R. W. Sinkeldam, K. J. Phelps, A. Fin, D. J. Tantillo, Y. Tor, P. A. Beal, *Angew. Chem. Int. Ed.* **2015**, *54*, 8713–8716.
[23] J. Kypr, I. Kejnovská, D. Renčiuk, M. Vorlíčková, *Nucleic Acids Res.* **2009**, *37*, 1713–1725.

Manuscript received: December 6, 2019
Revised manuscript received: January 24, 2020
Accepted manuscript online: January 24, 2020